High-Temperature Reactions of OH Radicals with Benzene and Toluene

Takamasa Seta, Masakazu Nakajima, and Akira Miyoshi*

Department of Chemical System Engineering, School of Engineering, The University of Tokyo, 7-3-1 Hongo, Bunkyo-ku, Tokyo 113-8656, Japan

Received: December 28, 2005; In Final Form: February 25, 2006

The rate constants for the reactions of OH radicals with benzene and toluene have been measured directly by a shock tube/pulsed laser-induced fluorescence imaging method at high temperatures. The OH radicals were generated by the thermal decomposition of nitric acid or *tert*-butyl hydroperoxide. The derived Arrhenius expressions for the rate constants were $k(\mathrm{OH} + \text{benzene}) = 8.0 \times 10^{-11} \exp(-26.6\ \mathrm{kJ\ mol^{-1}}/RT)$ [908−1736 K] and $k(\mathrm{OH} + \text{toluene}) = 8.9 \times 10^{-11} \exp(-19.7\ \mathrm{kJ\ mol^{-1}}/RT)$ [919−1481 K] in the units of cubic centimeters per molecule per second. Transition-state theory (TST) calculations based on quantum chemically predicted energetics confirmed the dominance of the H-atom abstraction channel for OH + benzene and the methyl-H abstraction channel for OH + toluene in the experimental temperature range. The TST calculation indicated that the anharmonicity of the C−H−O bending vibrations of the transition states is essential to reproduce the observed rate constants. Possible implications to the other analogous H-transfer reactions were discussed.

Introduction

Elucidation of the oxidation/formation mechanisms of the aromatic hydrocarbons is one of the most important research areas in combustion chemistry. The aromatic compounds are major constituents of practical fuels, and for example, their contents are ∼30% in gasoline and ∼20% in diesel fuel. Because of the high resistance toward autoignition, they are used as antiknock additives to enhance the octane number of gasoline. Also, the aromatic hydrocarbons are produced in combustion, even in the combustion of aliphatic fuels, and are known to play central roles in the mechanism of the formation of PAHs (polycyclic aromatic hydrocarbons) and particulate matters, or soot. However, the kinetic information is still limited for the reactions of aromatic hydrocarbons, especially at elevated temperatures, mainly due to the experimental difficulties.

The reactions of OH radicals with benzene and toluene

$$\mathrm{OH} + \mathrm{C_6H_6} \rightarrow \text{products} \quad (1)$$

$$\mathrm{OH} + \mathrm{C_6H_5CH_3} \rightarrow \text{products} \quad (2)$$

are important initial oxidation steps of benzene and toluene in combustion. Also, the reactions are important key reactions in PAH formation. For example, the C_6H_5 (phenyl) radical formed as one possible product by OH + benzene (reaction 1), produces the cyclopentadienyl (C_5H_5) radical, an important key species for aromatic ring growth, via subsequent reactions, $C_6H_5 + O_2 \rightarrow C_6H_5O + O$ and $C_6H_5O + M \rightarrow C_5H_5 + CO + M$.

Because they are also important in the atmospheric photooxidation processes, reactions 1 and 2 have been investigated extensively at around room temperature.[1−22] Under atmospheric conditions, they are known to proceed mainly via the formation of OH adducts, hydroxycyclohexadienyl radicals (C_6H_6OH and $HOC_6H_5CH_3$), though the subsequent oxidation mechanism is still controversial. The H-atom abstraction channels have been reported to be minor, ∼5% for OH + benzene and ∼10% for OH + toluene at room temperature.[3]

Because of the small binding energy, the OH−benzene or OH−toluene adduct is no longer stable at elevated temperatures. Lin et al.[23] observed the equilibrium reaction, $\mathrm{OH} + \mathrm{C_6H_6} \leftrightarrow \mathrm{C_6H_6OH}$, in the temperature range 345−385 K and derived the heat of reaction, $\Delta H\ (365 \pm 20\ \mathrm{K}) = -84 \pm 4\ \mathrm{kJ\ mol^{-1}}$. Though limited, a few kinetic studies have been also reported at higher temperatures.[24−27] Tully et al.[24] employed the flash photolysis−resonance fluorescence technique for the study of reactions 1 and 2 up to 1150 K. Madronich and Felder[25] determined the rate coefficient for reaction 1 over the temperature range 790−1410 K using the high-temperature photochemistry technique. It has been well-established that, as temperature increases, the apparent rate constant for reaction 1 or 2 steeply drops in the region around 350−400 K and starts to increase over ∼500 K.[26] This strange temperature dependence has been well-interpreted by the equilibrium around 350−400 K as observed by Lin et al.[23] and the opening of the H-abstraction channels above ∼500 K. The observed kinetic isotope effect for OH + benzene,[5,24] $k_1(\mathrm{H})/k_1(\mathrm{D}) \approx 2$, also supports the dominance of the H-abstraction channel for reaction 1 above 500 K. Further, Tully et al.[24] used partially deuterated toluenes for the elucidation of the mechanism of the reaction 2, and the side-chain H-abstraction channel has been shown to be predominant above 500 K.

Recently, Tokmakov and Lin[28] and Chen et al.[29] reported extensive theoretical investigations on the OH + benzene (reaction 1). The thermochemical properties of intermediates, OH adduct, and prereaction complex and the structures and properties of the important transition states were estimated by ab initio and density functional calculations. Their RRKM or QRRK calculations succeeded in reproducing the observed rate constants semiquantitatively and concluded that the H/OH-substitution channel at high temperatures is negligible. However, neither study reproduced the experimental rate constants accurately above 500 K. The slope of the Arrhenius plot seems to be significantly different. Considering the importance of the reaction in the combustion of benzene, as an initial oxidation step and as a possible key reaction in PAH formation, extension of the experimental and/or theoretical investigations is needed

* Corresponding author. E-mail address: miyoshi@chemsys.t.u-tokyo.ac.jp.

10.1021/jp0575456 CCC: $33.50
Published on Web 03/25/2006

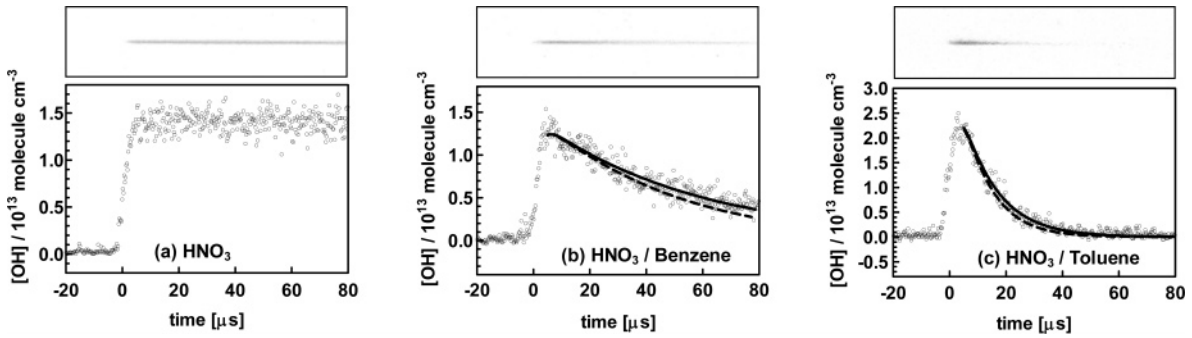

Figure 1. Observed PLIF images and derived [OH] time profiles for (a) $HONO_2$/Ar mixture, (b) $HONO_2$/benzene/Ar, and (c) $HONO_2$/toluene/Ar mixtures. Experimental conditions: (a) $T = 1455$ K, $P = 1.80$ atm, and $[HNO_3]_0 = 1.36 \times 10^{13}$ molecules cm^{-3}. (b) $T = 1451$ K, $P = 1.80$ atm, $[HNO_3]_0 = 1.38 \times 10^{13}$ molecules cm^{-3}, and $[C_6H_6]_0 = 1.87 \times 10^{15}$ molecules cm^{-3}. (c) $T = 1442$ K, $P = 1.79$ atm, $[HNO_3]_0 = 3.11 \times 10^{13}$ molecules cm^{-3}, and $[C_6H_5CH_3]_0 = 4.32 \times 10^{15}$ molecules cm^{-3}. The solid and broken lines denote the results of the numerical simulation with $k_8 = k_9 = 1 \times 10^{-10}$ and $k_8 = k_9 = 1 \times 10^{-9}$ cm^3 molecule^{-1} s^{-1}, respectively (see text for details).

for the high-temperature region. As for OH + toluene (reaction 2), theoretical calculations on the formation of OH adduct isomers have been reported by Suh et al.[30] No theoretical investigation including the H-abstraction channels has been reported so far.

In the present work, high-temperature reactions of OH radicals with benzene and toluene have been investigated by a shock tube/pulsed laser-induced fluorescence imaging method[31] developed recently in our laboratory. The kinetic measurements were extended to high temperatures up to 1736 K for OH + benzene and up to 1481 K for OH + toluene, in order to provide reliable experimental rate constants in the temperature range of combustion interest. The result for OH + benzene was analyzed by the transition-state theory (TST) based on quantum chemical calculations, in order to resolve the disagreement between the theory and the experiments. The reaction of OH + toluene was also analyzed on the basis of TST calculations.

Experimental Section

Experiments were carried out by a shock tube/pulsed laser-induced fluorescence imaging method (ST-PLIFI)[31] developed recently by the authors, and the details of the apparatus have been described elsewhere.[31] A brief description is given here. The PLIFI detection system is located at the end of the shock tube. An image of a laser-irradiated cylindrical fluorescing part of the shock-heated gas sample is focused upon the photocathode plate of an image intensifier (Hamamatsu V4436U) by ultraviolet focusing lenses. The intensified fluorescence image is digitized by a digital CCD camera. The OH radicals were excited at the overlapping $Q_1(1)$ and $R_2(3)$ lines of the A−X (1, 0) band at 281.99 nm. A band-pass filter with peak transmission at 310 nm and 5-nm fwhm was used to select the A−X (1, 1) band fluorescence of the OH radical. The probe laser light was generated by a XeCl excimer laser (Lambda Physik ComPex 102) pumped dye laser (Lambda Physik Scanmate 1) with a frequency doubler (Lambda Physik Scanmate UV). The typical laser pulse energy was ∼1 mJ at 281.99 nm by using coumarin 540A dye and a β-barium borate (BBO) frequency-doubling crystal.

The OH radicals were generated by the thermal decomposition of $HONO_2$ (gaseous nitric acid) or TBHP (*tert*-butyl hydroperoxide, $(CH_3)_3C-OOH$).

$$HONO_2 + M \rightarrow OH + NO_2 + M \quad (3)$$

$$(CH_3)_3C-OOH + M \rightarrow OH + (CH_3)_3C-O + M \quad (4)$$

The nitric acid was useful for temperatures above 1300 K, where it decomposes within a sufficiently short time ($<10^{-5}$ s) compared to the time scale of observation of reaction 1 or 2. For temperatures below 1300 K, TBHP was used for the OH-radical source, since it decomposes much more rapidly than the nitric acid and was useful down to 900 K.[32] The use of TBHP was limited below ∼1300 K, since it starts to decompose in the incident shock wave. It should be noted that the other dissociation product of TBHP, the *tert*-butoxy radical [$(CH_3)_3C-O$], rapidly decomposes to methyl radicals and acetone

$$(CH_3)_3C-O + M \rightarrow CH_3 + CH_3COCH_3 + M \quad (5)$$

and the effect of side reactions is relatively large in comparison to the case of $HONO_2$. Details of the secondary kinetics will be discussed in the following section.

The gaseous nitric acid was prepared by adding concentrated nitric acid (Wako, 70%) to two to three times the volume of concentrated sulfuric acid (Wako, 98%)[33] and was purified by trap-to-trap distillation. The sample containing TBHP was prepared by evaporating the aqueous solution of TBHP (Wako, 70%). The concentration of TBHP in the sample gas was estimated by assuming the ideal solution, which seems to be allowable since the vapor pressure of TBHP is similar to that of water. Ar (Nihon Sanso, 99.9999%), which was used as diluent throughout the present study, was purified by passage through a cold trap. He (Japan Helium Center, 99.9999%) for the driver gas was used without further purification. Benzene (Wako, 99.8%) and toluene (Katayama Chemical first grade, 99%) were purified by repeated trap-to-trap distillation cycles. The typical sample gas contained 1−4 ppm of OH-radical precursor ($HONO_2$ or TBHP) and 200−1100 ppm of benzene or toluene in Ar.

Results

A. Experiments Using $HONO_2$ for OH-Radical Source. Figure 1 shows three typical OH-PLIF images recorded with gas samples containing $HONO_2$ as the OH-radical source and derived concentration−time profiles of OH. Upon the arrival of reflected shock waves (time = 0), the OH radicals were generated nearly instantaneously and stayed at constant concentration during the observation period without hydrocarbon reactant (Figure 1a), while a decay of OH concentration was observed due to reaction 1 or 2 when benzene (Figure 1b) or toluene (Figure 1c) was added to the gas sample. The time variation of the fluorescence intensity was well-described by a single-exponential function

$$I(t) = I_0 \exp(-k't) \quad (E1)$$

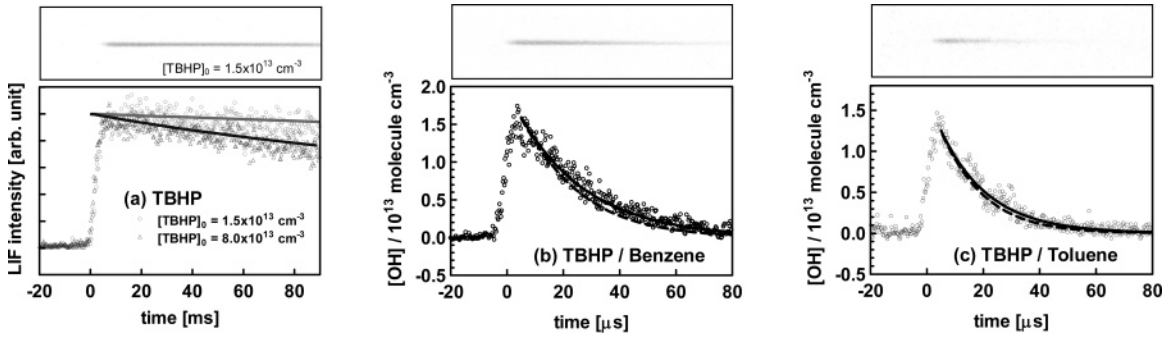

Figure 2. Observed PLIF images and derived [OH] time profiles for (a) TBHP/Ar mixture, (b) TBHP/benzene/Ar, and (c) TBHP/toluene/Ar mixtures. Experimental conditions: (a) $[TBHP]_0 = 1.5 \times 10^{13}$ (open circles, observed [OH]; solid gray line, simulated [OH]) and 8.0×10^{13} molecules cm^{-3} (open triangles, observed [OH]; solid black line, simulated [OH]). (b) $T = 1058$ K, $P = 1.08$ atm, $[TBHP]_0 = 1.94 \times 10^{13}$ molecules cm^{-3}, and $[C_6H_6]_0 = 8.49 \times 10^{15}$ molecule cm^{-3}. (c) $T = 1097$ K, $P = 1.14$ atm, $[TBHP]_0 = 1.67 \times 10^{13}$ molecules cm^{-3}, and $[C_6H_5CH_3]_0 = 5.16 \times 10^{15}$ molecules cm^{-3}. The solid and broken lines denote the results of the numerical simulation with $k_8 = k_9 = 1 \times 10^{-10}$ and $k_8 = k_9 = 1 \times 10^{-9}$ cm^3 molecule^{-1} s^{-1}, respectively (see text for details).

where I_0 is the fluorescence intensity at $t = 0$ and k' is the pseudo first-order decay rate of OH radicals. Since the experiments were performed under pseudo first-order conditions, that is, [benzene or toluene]$_0$/[OH]$_0$ = 130−440, the rate constant for reaction 1 or 2, k_1 or k_2, was derived from a simple relation, $k' = k_1[\text{benzene}]_0$ or $k' = k_2[\text{toluene}]_0$.

Although the absolute concentrations of OH radicals are not important in the pseudo first-order analysis, they are needed for the assessment of the possible effect of side reactions, most of which are radical−radical reactions. The absolute OH-radical concentration was evaluated by assuming $[OH]_0 = [HONO_2]_0$, since the nitric acid is known to dissociate to OH + NO_2 quantitatively.[34] The typical initial concentration of OH radicals was around 2×10^{13} molecules cm^{-3}. Possible side reactions of the species originating from $HONO_2$ are as follows:

$$OH + NO_2 \rightarrow HO_2 + NO \quad (6)$$

$$OH + OH \rightarrow H_2O + O \quad (7)$$

The contribution of these reactions can be readily excluded from the time profile in Figure 1a, which was observed without benzene or toluene since no decay of [OH] was visible. This can also be confirmed from the rate constants for these reactions, that is, by using $k_6 = 2 \times 10^{-12}$, $k_7 = 5 \times 10^{-12}$ (both in units of cm^3 molecule^{-1} s^{-1} and at 1500 K),[35,36] and the maximum possible concentration of NO_2 and OH, $\leq [HONO_2]_0 \approx 2 \times 10^{13}$ molecules cm^{-3}. Their contributions to the first-order decay were estimated to be 40 s^{-1} and 100 s^{-1}, respectively, which are less than 1% of the observed decay rate, typically $(2-8) \times 10^4$ s^{-1}.

The dominant channels of reactions 1 and 2 are expected to be H-atom abstraction reactions (1a and 2a) at high temperatures. The minor substitution channels (1b, 2c, and 2d) and ring H-abstraction channel (2b), which will be discussed in the following section, are neglected here.

$$OH + C_6H_6 \rightarrow C_6H_5 + H_2O \quad (1a)$$

$$OH + C_6H_5CH_3 \rightarrow C_6H_5CH_2 + H_2O \quad (2a)$$

The most significant side reactions will be the reactions of OH radicals with the reaction products.

$$OH + C_6H_5 \rightarrow \text{products} \quad (8)$$

$$OH + C_6H_5CH_2 \rightarrow \text{products} \quad (9)$$

Since no direct kinetic measurement has been reported for these reactions, possible interference was evaluated by numerical simulation by varying the rate constants for these reactions. The reactions used in the numerical simulation are listed in Table 1S (Supporting Information). Although other reaction products, three isomers of methyl phenyl radicals, can be expected for OH + toluene, and the products may decompose further to other species such as benzyne and its derivatives, these are represented by a single species C_6H_5 or $C_6H_5CH_2$ in the numerical simulation. The distinction of these species makes no practical difference because of the lack of their rate constants with OH radical.

The calculated OH radical concentrations are compared with experiments in Figure 1b,c. The solid lines show the calculations with k_8 (or k_9) = 1×10^{-10} cm^3 molecule^{-1} s^{-1} (typical rate constant for radical−radical reactions), while broken lines denote those with 1×10^{-9} cm^3 molecule^{-1} s^{-1} (estimated maximum rate constant ≈ gas kinetic collision rate constant). The effect of reaction 8 or 9 was found to be minor, though it was slightly larger for the OH + benzene experiment (Figure 1b) than for OH + toluene (Figure 1c), reflecting the smaller rate constant for reaction 1 than that for reaction 2. Furthermore, a trial was also made to investigate the rate constant, k_8, for OH + C_6H_5 (reaction 8) by separate experiments using nitrosobenzene (C_6H_5-NO) as a pyrolytic source of phenyl radical. The upper limit for k_8 was evaluated to be $\sim 10^{-10}$ cm^3 molecule^{-1} s^{-1}. This indicated that the contribution of reaction 8 was sufficiently small in the present experimental conditions. Other side reactions were also concluded to be negligible by the numerical simulations.

B. Experiments using TBHP. Since $HONO_2$ is useful as an OH radical source only for temperatures above ~1300 K, measurements were extended to lower temperatures by using TBHP. Figure 2 shows typical fluorescence images and time profiles of [OH]. Similarly to Figure 1, Figure 2a−c indicates the results without reactants, with benzene, and with toluene, respectively. Unlike the case of $HONO_2$, a slight decay of [OH] was observed even in the absence of reactants (Figure 2a), mainly due to the subsequent reactions of OH radicals with the dissociation products of $(CH_3)_3C-O$ radicals, acetone (CH_3COCH_3), and CH_3 radicals.

$$OH + CH_3COCH_3 \rightarrow \text{products} \quad (10)$$

$$OH + CH_3 \rightarrow \text{products} \quad (11)$$

By using the rate constants for reactions 10[37] and 11[38] at 1200 K, $k_{10} = 9 \times 10^{-12}$ and $k_{11} = 2.7 \times 10^{-11}$ cm^3 molecule^{-1} s^{-1}, and $[CH_3COCH_3]_{max} = [CH_3]_{max} = [TBHP]_0 \sim 2 \times 10^{13}$

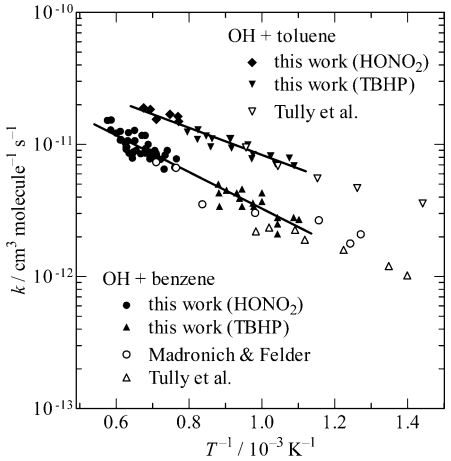

Figure 3. Arrhenius plots for the rate constants for OH + benzene and toluene in the high-temperature region. The symbols in lower left legend are measurements for OH + benzene (● and ▲, present studies with $HONO_2$ and TBHP, respectively; ○, Madronich and Felder;[25] △, Tully et al.[24]), and those in the upper right legend are measurements for OH + toluene (◆ and ▼, present studies with $HONO_2$ and TBHP, respectively; ▽, Tully et al.[24]). Solid lines correspond to the Arrhenius expressions, derived in the present work.

molecules cm^{-3}, contributions to the [OH] decay rate were estimated to be 180 and 540 s^{-1}, respectively, both of which are less than 2% of the measured decay rates of OH, (3−6) × 10^4 s^{-1}. To confirm the estimated mechanism, an experiment was also performed with about five times larger TBHP concentration, and the result is also shown in Figure 2a. The decay rate was found to increase as expected, and the profiles could be fairly well reproduced by the numerical simulation. To avoid the effect of these reactions, experiments were performed with lowest possible concentration of TBHP, ∼2 × 10^{13} molecules cm^{-3}.

Similar to the case of $HONO_2$ experiments, numerical simulations were performed by using the reactions listed in Table 2S (Supporting Information), and the time profiles calculated for two cases with k_8 (or k_9) = 1 × 10^{-10} and 1 × 10^{-9} cm^3 molecule^{-1} s^{-1} are shown in Figure 2b,c by solid and broken lines, respectively. The effect of side reactions 8 and 9 was confirmed to be negligible.

C. Temperature Dependence of the Rate Constants. The measured rate constants are summarized in Table 3S (Supporting Information) with experimental conditions and are shown in the Arrhenius plots (Figure 3). The rate constants for OH + toluene (reaction 2) were found to be two to three times larger than those for OH + benzene (reaction 1). No significant difference was found between the results with $HONO_2$ and TBHP. By a least-squares analysis, Arrhenius rate constant expressions for reactions 1 and 2 were derived to be (in units of cm^3 molecule^{-1} s^{-1})

$$k_1 = (8.0 \pm 1.7) \times 10^{-11} \times \exp\{-(26.6 \pm 2.0[\text{kJ mol}^{-1}])/RT\} \qquad F = 1.32 \quad (908-1736\ \text{K})$$

$$k_2 = (8.9 \pm 2.9) \times 10^{-11} \times \exp\{-(19.7 \pm 2.7[\text{kJ mol}^{-1}])/RT\} \qquad F = 1.20 \quad (919-1481\ \text{K})$$

Here, the error limits for preexponential factor and activation energy are at the two standard deviation (2σ) level. F is the uncertainty factor (also, at the 2σ level) of the rate constants in the specified temperature range. The present results for reactions 1 and 2 agree well with those of Tully et al.[24] and Madronich and Felder.[25] Derived activation energies are slightly larger (by 5−8 kJ mol^{-1}) than those reported in the earlier works for the lower temperature range, suggesting non-Arrhenius behavior of the rate constants.

Discussion

For the reaction of OH radicals with benzene (reaction 1), previous extensive theoretical analyses[28,29] have clearly established the mechanism based on the experimental kinetic data. However, the agreement between experimental and theoretical rate constants was not satisfactory at temperatures above ∼500 K. In the present study, previous high-temperature rate constants for OH + benzene have been confirmed and extended up to 1740 K. Since this reaction is an important initial oxidation step for the simplest aromatic hydrocarbon, the theoretical investigation was also extended in the present study in order to resolve the discrepancy. A theoretical investigation was also made for the reaction of OH radicals with toluene (reaction 2).

A. Energetics of OH + Benzene and OH + Toluene Reaction Systems. The energetics of the reaction systems were estimated from the experimental heats of formation, the estimates proposed in the previous theoretical investigations, and quantum chemical calculations of G3(MP2)//B3LYP[39] and CBS-QB3[40] models carried out using the *Gaussian 98* or *03* programs.[41] Although the previous studies seem to have well-established the dominance of the H-abstraction channel (reaction 1a) for OH + benzene at high temperatures, the barrier for the H/OH-substitution reaction 1b was estimated to lie only 10−20 kJ mol^{-1} above that of the H-abstraction channel, and this channel may contribute significantly at elevated temperatures.

$$\text{OH} + \text{C}_6\text{H}_6 \rightarrow \text{C}_6\text{H}_5 + \text{H}_2\text{O} \quad (1a)$$

$$\rightarrow \text{C}_6\text{H}_5\text{OH (phenol)} + \text{H} \quad (1b)$$

Thus, the quantum chemical calculations were made for both channels. Other reaction channels, which have been extensively investigated by Chen et al.,[29] were excluded, since the barrier heights were reported to be much higher, by at least 50 kJ mol^{-1}, than that for the H-abstraction channel. Similarly, for OH + toluene (reaction 2), four H-abstraction channels (reactions 2a, 2b-*o*, 2b-*m*, and 2b-*p*) and four substitution channels (reactions 2c, 2d-*o*, 2d-*m*, and 2d-*p*) have been investigated. The calculated

$$\text{OH} + \text{C}_6\text{H}_5\text{CH}_3 \rightarrow \text{C}_6\text{H}_5\text{CH}_2 + \text{H}_2\text{O} \quad (2a)$$

$$\rightarrow o\text{-}, m\text{-}, p\text{-C}_6\text{H}_4\text{CH}_3 + \text{H}_2\text{O} \quad (2b\text{-}o, 2b\text{-}m, 2b\text{-}p)$$

$$\rightarrow \text{C}_6\text{H}_5\text{OH} + \text{CH}_3 \quad (2c)$$

$$\rightarrow o\text{-}, m\text{-}, p\text{-C}_6\text{H}_4\text{CH}_3\text{OH (cresol)} + \text{H} \quad (2d\text{-}o, 2d\text{-}m, 2d\text{-}p)$$

internal energy at 0 K relative to the reactants, E_{rel}(0 K), are summarized and compared with experimental thermodynamic data and previous estimations in Table 1. The last column of the table shows the best estimates of E_{rel}(0 K), which are used in the TST calculations described in the following subsection. For OH + benzene, the best-estimate energetics for H/OH-substitution steps were taken from the previous work by Tokmakov and Lin,[28] who have chosen these so as to reproduce the reported rate constants for OH + benzene at low temperatures, as well as those for reverse OH/H-substitution reaction,

TABLE 1: Estimated Energetics for OH + C_6H_6/$C_6H_5CH_3$ Systems

E_{rel}(0 K)[a]/kJ mol^{-1}	G3(MP2)//B3LYP	CBS-QB3	exp.[b]	Tokmakov & Lin[c]	TST fit[d]	best est.[e]
			OH + C_6H_6 (benzene) system			
OH + benzene (C_6H_6)	0	0	0	0	0	0
TSabs	32.5	14.7			12	12.0
H_2O + phenyl (C_6H_5)	−12.1	−16.6	−23.0			−23.0
vdW (OH···C_6H_6)				−10.9		−10.9
TSadd	18.4	2.1		0.4		0.4
adduct (C_6H_6OH)	−52.7	−67.5		−71.1		−71.1
TSelim	53.5	38.5		34.7		34.7
H + phenol (C_6H_5OH)	7.9	1.1	1.3	1.3		1.3
			OH + $C_6H_5CH_3$ (toluene) System			
OH + toluene ($C_6H_5CH_3$)	0	0	0		0	0
TSabs-CH_3	11.6	5.2			2.5	2.5
H_2O + benzyl ($C_6H_5CH_2$)	−107.1	−119.1	−122.8			−122.8
TSabs-*o*	25.4	12.6				9.9[f]
TSabs-*m*	27.8	15.5				12.8[f]
TSabs-*p*	29.7	13.9				11.2[f]
H_2O + *o*-CH_3−Phenyl	−12.3	−20.2				−26.5[g]
H_2O + *m*-CH_3−Phenyl	−12.3	−20.4				−26.7[g]
H_2O + *p*-CH_3−Phenyl	−9.8	−15.5				−21.8[g]
vdW (OH···$C_6H_5CH_3$)						−10.9[h]
TSadd-*ipso*	12.4	−4.3				−4.3
ipso-adduct (*ipso*-$HOC_6H_5CH_3$)	−71.4	−86.0				−86.0
TSelim-*ipso*	35.6	18.5				18.5
CH_3 + phenol (C_6H_5OH)	−33.2	−36.2	−37.9			−37.9
TSadd-*o*	11.1	−4.6				−6.3[i]
TSadd-*m*	18.0	0.7				−1.0[i]
TSadd-*p*	16.6	−0.4				−2.1[i]
o-adduct (*o*-$HOC_6H_5CH_3$)	−67.0	−82.6				−86.2[j]
m-adduct (*m*-$HOC_6H_5CH_3$)	−62.6	−77.4				−81.0[j]
p-adduct (*p*-$HOC_6H_5CH_3$)	−63.5	−79.0				−82.6[j]
TSelim-*o*	46.2	30.8				27.0[k]
TSelim-*m*	53.4	37.0				33.2[k]
TSelim-*p*	54.7	38.7				35.0[k]
H + *o*-cresol (*o*-$HOC_6H_4CH_3$)	5.5	−2.1	1.1			1.1
H + *m*-cresol (*m*-$HOC_6H_4CH_3$)	12.2	0.9	−1.9			−1.9
H + *p*-cresol (*p*-$HOC_6H_4CH_3$)	9.7	2.4	5.0			5.0

[a] All energies reported here, E_{rel}(0 K), are the internal energies at 0 K relative to the reactants, OH + benzene or OH + toluene, in kJ mol^{-1}. [b] Experimental E(0 K) was derived from experimental $\Delta_f H_{298}$ and $H_{298} - H_0$ calculated from the B3LYP/6-31G(d) optimized geometry and frequencies. For OH, experimental spin−orbit splitting was used, and for toluene and cresols, −CH_3 group was treated as a hindered rotor. Experimental $\Delta_f H_{298}$ values were taken from thermodynamic tables,[42−44] except for OH,[45] CH_3,[46] and phenyl,[47] for which revised heats of formation have been reported recently. [c] Energetics used by Tokmakov and Lin[28] in their final rate-constant evaluation. [d] Derived by the best fit to the experimental rate constants measured in this study. See text for details. [e] Best estimates evaluated in the present study. [f] Estimated as E(CBS-QB3) − 2.73 kJ mol^{-1}, based on the difference between TST fit (best estimate) and CBS-QB3 energies for H-atom abstraction transition state of OH + benzene. [g] Estimated as E(CBS-QB3) − 6.34 kJ mol^{-1}, based on the difference between experimental and CBS-QB3 energies for H_2O + phenyl (C_6H_5). [h] Estimated to be same as vdW (OH···C_6H_6). [i] E(CBS-QB3) − 1.68 kJ mol^{-1}. [j] E(CBS-QB3) − 3.59 kJ mol^{-1}. [k] E(CBS-QB3) − 3.76 kJ mol^{-1}.

H + C_6H_5OH → OH + C_6H_6. The height of TS_{abs}, transition state for the H-abstraction channel, was adjusted so as to reproduce the high-temperature rate constants determined in the present and previous[24,25] studies. Details of this procedure will be described below. It should be noted that the CBS-QB3 model reproduces the experimental and best estimated energetics quite well. The differences were only ∼3 kJ mol^{-1} on average and 6.3 kJ mol^{-1} at maximum. The best-estimate energy diagram for the OH + benzene system is shown in Figure 4.

For the OH + toluene system, experimental thermochemical information is available only for the methyl H-abstraction products (H_2O + benzyl) and substitution products (CH_3 + phenol and H + cresol). Again, because the CBS-QB3 model well-predicted the experimental relative energies of these products, the unknown energetics were estimated from the CBS-QB3 results. Since the CBS-QB3 model overestimated the E_{rel}(0 K) of H_2O + phenyl by 6.3 kJ mol^{-1}, the E_{rel}(0 K) values of aromatic ring H-abstraction products, H_2O + *o*-, *m*-, and *p*-methyl phenyl radical, were estimated by shifting the CBS-QB3 energy lower by 6.3 kJ mol^{-1}. Similarly, the height of ring H-abstraction transition states, TS_{abs-o}, TS_{abs-m}, and TS_{abs-p}, were estimated as E(CBS-QB3) − 2.7 kJ mol^{-1}. A similar procedure was applied to the OH/H-substitution channels, but not for the *ipso*-OH/CH_3-substition channel, for which CBS-QB3 energies were used without shifting. The barrier height for the methyl H-abstraction channel, which is most sensitive to the rate constants at high temperatures, was adjusted so as

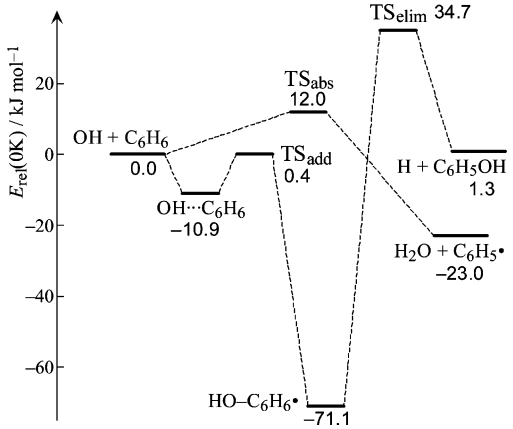

Figure 4. Estimated energy diagram for the OH + benzene system. The ordinate, E_{rel}(0 K), is the internal energy at 0 K (in other words, the potential energy corrected for the zero-point vibrational energy) relative to the reactant, OH + benzene. See text and footnotes of Table 1 for details.

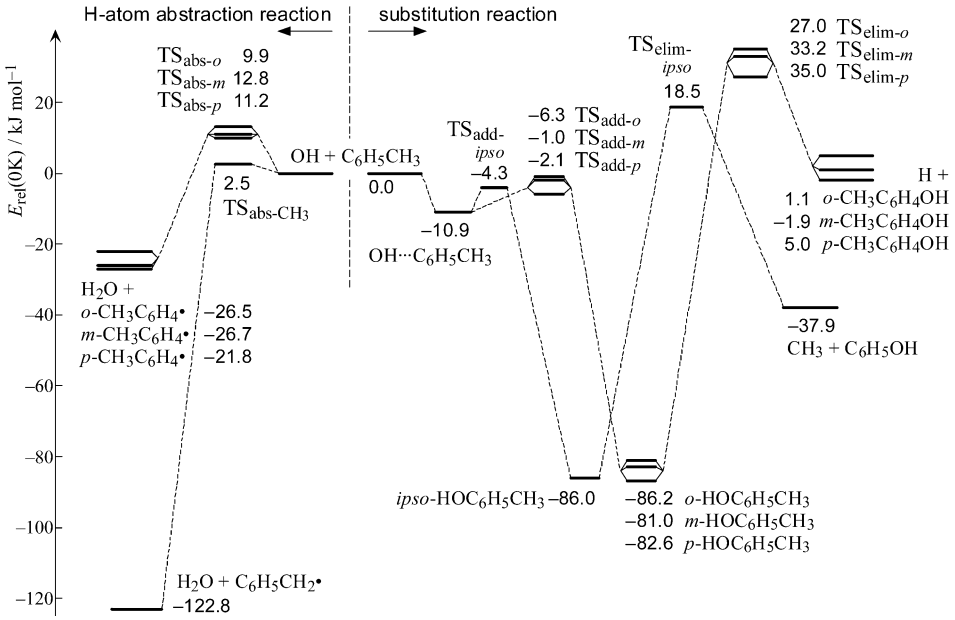

Figure 5. Estimated energy diagram for the OH + toluene system. The ordinate, E_{rel}(0 K), is the internal energy at 0 K relative to the reactant, OH + toluene. For detail of the estimation procedure, see text as well as footnotes of Table 1.

to reproduce the present and previous measurements (see following subsection for detail). The best-estimate energetics for the OH + toluene system is shown in Figure 5.

The $OH\cdots C_6H_6$ and $OH\cdots C_6H_5CH_3$ van der Waals (vdW) complexes are also shown in Table 1 and Figures 4 and 5 based on the calculation by Tokmakov and Lin.[28] For addition or insertion reactions without high entrance barriers, such complexes are known to be important in the theoretical treatment of the rate constants at low temperatures.[28,48] However, their roles are minor at high temperatures, and no further investigation was made for these complexes in the present study.

B. TST (Transition-State Theory) Calculations. Molecular properties required for the TST calculations, structures, and vibrational frequencies, were estimated by B3LYP/6-31G(d) density functional calculations. The optimized structures of reactants, products, intermediates, and transition states are shown in Figures 1S and 2S (Supporting Information), and properties used in the TST calculations are summarized in Tables 4S and 5S. Since the methyl torsion of toluene was found to have an extremely low vibrational frequency, 30.6 cm^{-1}, and a low barrier, 6.7 cm^{-1}, by B3LYP/6-31G(d) calculations, its partition function was calculated by assuming a sinusoidally hindered rotor with sixfold symmetry by using the Pitzer−Gwinn approximation.[49] The methyl torsion modes of OH + toluene transition states and products were treated similarly except for the methyl H-abstraction transition state. The spin−orbit splitting of the $^2\Pi$ ground state of the OH radical was incorporated in the calculation by using the experimental coupling constant,[50] $A_0 = -139.21$ cm^{-1}, for the vibrational ground state. The molecular models thus estimated were confirmed by comparing the calculated entropies and heat capacities with experimental values, if available, as shown in Table 6S. The one-dimensional tunneling correction was applied to the canonical TST rate constants by assuming an asymmetric Eckart potential,[51] though the effect was found to be minor at high temperatures.

The benzene−OH or toluene−OH adducts, which are dominant products at low temperatures, are not likely to be formed and stabilized as a product under high-temperature conditions in the present study, because the binding energies are estimated to be small, 71−86 kJ mol^{-1}. Since the H-elimination or CH_3-elimination barriers (18−35 kJ mol^{-1}) are higher than the OH-addition barriers (−6−1 kJ mol^{-1}), it is reasonable to assume pre-equilibrium between the reactants and the OH adduct. In this situation, TST rate constants for the substitution channel, k_{sub}, become

$$k_{sub} = K \times k_{elim} = \frac{Q_{ad}}{Q_r}\exp\left(\frac{D_0}{k_B T}\right) \times \kappa \frac{k_B T}{h}\frac{Q^*_{elim}}{Q_{ad}}\exp\left(-\frac{E_0}{k_B T}\right)$$
$$= \kappa \frac{k_B T}{h}\frac{Q^*_{elim}}{Q_r}\exp\left(-\frac{E_0 - D_0}{k_B T}\right) \qquad \text{(E2)}$$

where K is the equilibrium constant between the reactants and the OH adduct, k_{elim} is the rate constant for the H-elimination (or CH_3-elimination) step, κ is the tunneling correction factor; Q_r, Q_{ad}, and Q^*_{elim} are the partition functions of the reactants, the OH adduct, and the H-elimination transition state; D_0 is the backward dissociation energy of the OH adduct to reactants, and E_0 is the threshold energy for the H-elimination reaction. Note that eq E2 is the same as the TST rate constant derived by ignoring the OH adduct, except that the parameters for the Eckart potential used to evaluate κ are determined for the H-elimination step from the OH adduct.

C. Rate Constant for OH + Benzene. The rate constant for the H/OH-substitution channel, $OH + C_6H_6 \rightarrow C_6H_5OH + H$ (reaction 1b), was calculated by eq E2 with the best-estimate E_{rel}(0 K) in Table 1. The result is shown in Figure 6 by a dotted broken line, and the H/OH-substitution channel was confirmed to be minor; that is, it is less than 10% of the measured rate constant. Then, the rate constant for the dominant H-abstraction channel, $OH + C_6H_6 \rightarrow C_6H_5 + H_2O$ (reaction 1a), was calculated with the harmonic oscillator (HO) approximation for all internal motions of the transition state (HO model). The barrier height was adjusted so that the calculated total rate constant reproduces the experiments. However, as shown by a broken line in Figure 6, the HO model did not reproduce the temperature dependence of the experimental rate constant properly, and the derived threshold energy, $E_0 = 24$ kJ mol^{-1}, was significantly higher than the CBS-QB3 estimate (14.7 kJ mol^{-1}; see Table 1). Since such disagreement is often caused by the overestimated partition function of the transition state

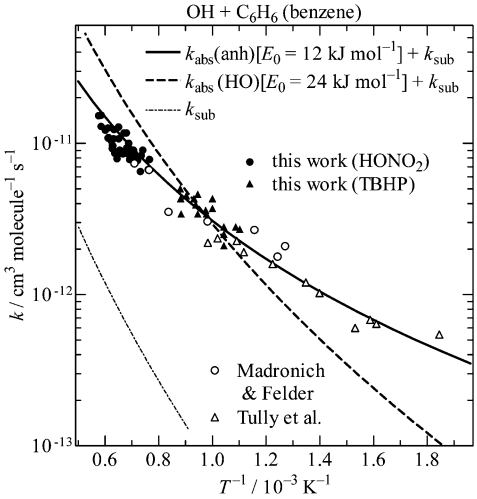

Figure 6. Comparison of the TST calculations with experimental rate constants for OH + benzene. The symbols denote the experimental rate constants (see the caption of Figure 3 for their legends). The solid (—) and broken (- - - -) lines show the overall TST rate constant calculated with and without one-dimensional anharmonic corrections for two bending and one torsional vibration of the transition state, respectively. The estimated rate constant for the H/OH-substitution channel is also shown by the dotted broken line (-·-·-).

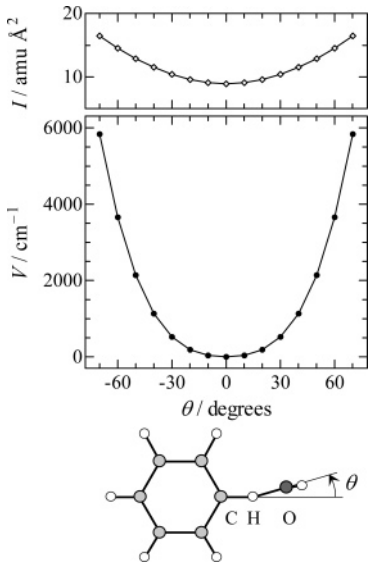

Figure 7. Variation of the potential energy, *V*, (middle trace) and the reduced moment of inertia, *I*, (upper trace) along the C−H−O wagging (*a*″-bending) vibration coordinate, θ, of the H-abstraction transition state for OH + benzene, estimated by B3LYP/6-31G(d) density functional calculations. Definition of the wagging coordinate, θ, is shown schematically in the bottom.

due to improper harmonic oscillator approximation, three low-frequency vibrational modes, C−H−O wagging (*a*″ bending), C−H−O rocking (*a*′ bending), and −OH torsion, were investigated in detail.

Figure 7 shows a potential energy curve for the C−H−O wagging vibration of the H-abstraction transition state estimated by B3LYP/6-31G(d) calculations. The potential curve is highly anharmonic, and the reduced moment of inertia depends significantly on the bending coordinate. The reduced moment of inertia for the C−H−O bending vibration was calculated by the same protocol as for the asymmetric internal rotor described by Pitzer,[52] except that the axis of rotation is set to pass through the center H atom and perpendicular to the C−H−O bending plane. The bending coordinate, θ, was transformed to the inertia-weighted coordinate, ϕ, by

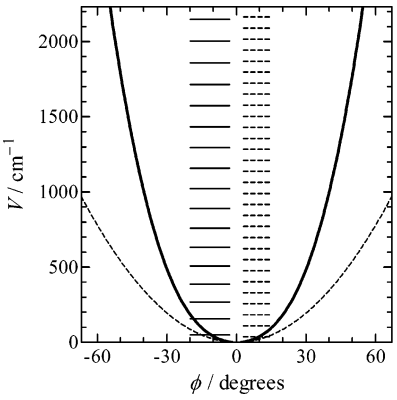

Figure 8. Potential energy curve along the inertia-weighted C−H−O wagging (*a*″-bending) vibration coordinate, ϕ, (solid curve, —) based on B3LYP/6-31G(d) calculations, and the energy levels of the vibrational states (horizontal solid lines, —) of the H-abstraction transition state for OH + benzene. The broken curve (- - -) and the broken horizontal lines (- - -) show the potential energy curve and the energy levels, respectively, for the harmonic oscillator approximation based on the conventional frequency analysis, that is, the frequency estimated from the second derivative of the potential energy at the minimum.

$$d\phi = (I/I_0)^{1/2}\, d\theta \qquad \text{(E3)}$$

where, I_0 is the reduced moment of inertia at the equilibrium geometry. Then, the vibrational energy levels were calculated by solving the time-independent Schrödinger equation, $-(\hbar^2/2I_0)(d^2\psi/d\phi^2) + V(\phi)\psi = E\psi$, with the BEx1D program.[53] The potential energy curve along the inertia-weighted coordinate, ϕ, and the derived energy levels are shown in Figure 8. The potential energy and the energy levels were significantly different from those estimated from the frequency analysis, which are also shown in Figure 8 by broken lines for comparison. The partition function was calculated directly from the energy levels.

Similarly, the partition functions for C−H−O rocking (*a*′ bending) and −OH torsion vibrations were calculated from the energy levels obtained by solving the Schrödinger equation. For the torsion vibration, the I_0 for inertia weighting was chosen as

$$I_0^{1/2} = \frac{1}{2\pi}\int_0^{2\pi} I^{1/2}\, d\theta \qquad \text{(E4)}$$

by which the intuitive and convenient periodicity is retained, because $\phi = 2\pi$ at $\theta = 2\pi$.

By using the partition functions derived above, TST calculation well-reproduced the experimental rate constant, as shown by the solid line in Figure 6. The derived threshold energy, $E_0 = 12$ kJ mol^{-1}, was also reasonable, being slightly smaller than the CBS-QB3 estimate, 14.7 kJ mol^{-1}. It should be noted that the theoretical investigations by Tokmakov and Lin[28] and Chen et al.[29] did include similar anharmonic correction for the −OH torsion vibration. However, the effect on the partition function was not large for the −OH torsion vibration. The correction factor, (that is, the ratio of the anharmonic partition function to that calculated by harmonic oscillator approximation using frequency analysis results), *Q*(anh)/*Q*(HO), was 0.79−0.95 (1800−500 K) for −OH torsion, while it was 0.43−0.53 for C−H−O rocking and 0.55−0.62 for C−H−O wagging in the same temperature range. The anharmonicity of the two C−H−O bending vibrations was essential for the reproduction of the experimental rate constants by TST.

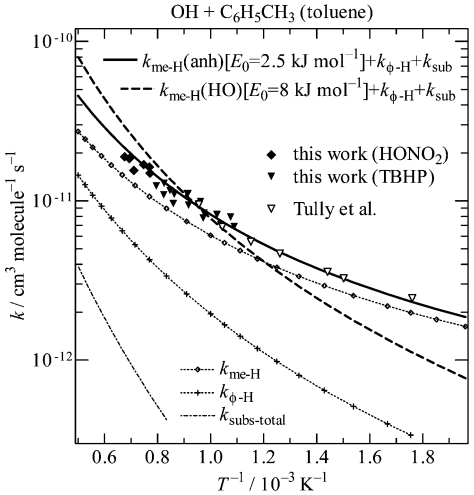

Figure 9. Comparison of the TST calculations with experimental rate constants for OH + toluene. The symbols denote the experimental rate constants (see the caption of Figure 3 for their legends). The solid (—) and broken (- - -) lines show the overall TST rate constant calculated with and without one-dimensional anharmonic corrections for one bending and two torsional vibrations of the transition state, respectively. The dotted line with open rhombus (···◇···◇···) indicates the rate constants for methyl H-abstraction channel, and the dotted line with crosses (···+···+···) denotes the sum of the rate constants for aromatic ring H-abstraction channels. The total rate constant for the four substitution channels is shown by the dotted broken line (-·-·-).

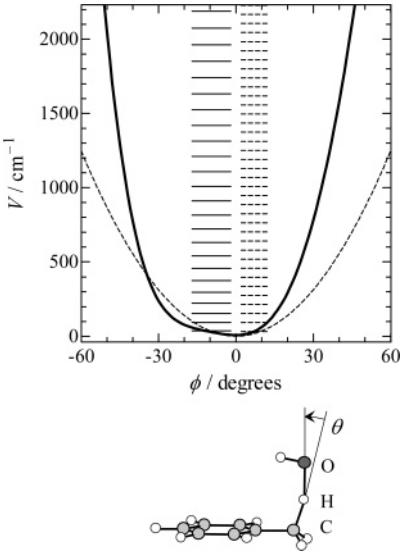

Figure 10. Potential energy curve along the inertia-weighted C−H−O rocking (a'-bending) vibration coordinate, ϕ, (solid curve, —) based on B3LYP/6-31G(d) calculations, and the energy levels of the vibrational states (horizontal solid lines, —) of the methyl H-abstraction transition state for OH + toluene. The broken curve (- - -) and the broken horizontal lines (- - -) show the potential energy curve and the energy levels, respectively, for the harmonic oscillator approximation based on the conventional frequency analysis. Definition of the rocking coordinate, θ, is shown in the bottom figure.

D. Rate Constant for OH + Toluene. The TST rate constants for all four substitution channels of OH + toluene (reaction 2) were calculated by eq E2. The sum of the rate constants for substitution channels is shown in Figure 9 by a dotted broken line and was confirmed to be minor as in the similar case, OH + benzene. Rate constants for the three (*ortho-*, *meta-*, and *para-*) aromatic-ring H-atom abstraction channels were calculated by the harmonic oscillator approximation and corrected by multiplying the anharmonic correction factor, Q(anh)/Q(HO), calculated for OH + benzene. The sum of the rate constants for three ring H-abstraction reaction channels is also shown by a dotted line with crosses in Figure 9, which was larger than that for substitution channels, but was still minor, less than 30% of the experimental overall rate constant. The barrier height for the major reaction channel, H abstraction from the CH_3 group, was adjusted so that the total rate constants agree with the experiments. The harmonic oscillator model cannot reproduce the temperature dependence of the rate constant, as shown by broken line in Figure 9.

The potential energy curves for the three internal motions corresponding to the three lowest vibrational frequencies of the methyl H-abstraction transition state were investigated by B3LYP/6-31G(d) calculations. The calculated potential energy curve and the vibrational energy levels for the C−H−O rocking (a'-bending) mode are shown in Figure 10. Obviously, the harmonic approximation based on the frequency analysis results in a significant overestimate of the partition function. Thus, the partition functions were evaluated from the energy levels. Similar calculations were also done for the −OH torsion mode and the C_6H_5−CH_3(OH) torsion. After correction for anharmonics, the TST rate constant agreed well with the experiments as shown in Figure 9. The best-fit threshold energy was derived to be, $E_0 = 2.5$ kJ mol^{-1}, which is slightly smaller than, but in good agreement with, the CBS-QB3 estimate, 5.2 kJ mol^{-1}. Unlike the case of OH + benzene, the −OH torsion is nearly a free rotor with a barrier less than 70 cm^{-1}. The major anharmonicity originated from the −OH torsion and the C−H−O rocking.

E. Effect of the Anharmonic Vibrations. The present direct experimental investigation at high temperatures, along with the theoretical investigation, indicates the importance of the anharmonic vibrational motions in the transition state. Although similar problems are well-known for the loose transition states of bond-fission reactions[54] and have also been pointed out for H-abstraction reactions,[55] no quantitative approach based on the quantum chemical calculations has been reported for H-abstraction reactions. Although the experimental rate constants may be reproduced parametrically by adjusting the relevant vibrational frequencies and/or by assuming a two-dimensional spherically hindered rotor with an adjustable hindrance angle, the anharmonicity was incorporated as a priori as possible in the present study. The experimental rate constants could be well-reproduced by only slight adjustment of the barrier height from the CBS-QB3 result, though it should be noted that further precise investigations are necessary for the problems arising from the limited accuracy of the potential energy calculation (at B3LYP/6-31G(d)) and the one-dimensional assumption ignoring the possible coupling between the internal motions, and so forth.

Because similar bending vibrations are expected in many other H-atom abstraction reactions from hydrocarbons, considerations on the possible effect of the anharmonicity seem to be useful. The effect of the anharmonicity of the bending vibrations was found to be larger for OH + benzene (reaction 1) than for OH + toluene (reaction 2). The major reason for this difference can be explained as follows: In the OH + toluene transition state, the coupling between the C−H−O wagging (a''-bending) and the −CH_3 torsion results in two normal modes: One is the in-phase torsion, in which the −CH_3(OH) rotates as a whole against the phenyl group, and the other is the reversed-phase torsion, in which nearly only the −CH_3 group rotates against the rest of the molecule, with OH staying still. As a result, the reduced mass of the latter normal mode, which dominantly

TABLE 2: Recommended Rate Constants for OH + Benzene and OH + Toluene (700−1900 K)[a]

		$k = AT^b \exp(-E_a/RT)$		
		A cm^3 molecule^{-1} s^{-1}	b	E_a/R K
	OH + Benzene			
k_1	$= k_{1a} + k_{1b}$	7.33×10^{-21}	2.907	231
k_{1a} (H-abstraction)		3.88×10^{-20}	2.683	369
k_{1b} (H/OH-substitution)		2.20×10^{-22}	3.249	2813
	OH + Toluene			
k_2	$= k_{2a} + k_{2b} + k_{2c} + k_{2d}$	2.52×10^{-20}	2.779	−405
k_{2a} (methyl-H-abstraction)		2.94×10^{-19}	2.394	−303
k_{2b} (ring-H-abstraction)	$= k_{2b-o} + k_{2b-m} + k_{2b-p}$	2.26×10^{-20}	2.691	312
k_{2b-o}	(*ortho*-H-abstraction)	8.57×10^{-21}	2.611	156
k_{2b-m}	(*meta*-H-abstraction)	1.23×10^{-20}	2.691	464
k_{2b-p}	(*para*-H-abstraction)	7.36×10^{-21}	2.665	305
k_{2c} (CH_3/OH-substitution)	*ipso*-	1.30×10^{-21}	2.884	1621
k_{2d} (ring-H/OH-substitution)	$= k_{2d-o} + k_{2d-m} + k_{2d-p}$	5.21×10^{-23}	3.365	2375
k_{2d-o}	(*ortho*-substitution)	2.74×10^{-23}	3.263	2071
k_{2d-m}	(*meta*-substitution)	7.34×10^{-23}	3.244	2667
k_{2d-p}	(*para*-substitution)	4.37×10^{-23}	3.231	2901
$k_{subs-total}$	$= k_{2c} + k_{2d}$	5.39×10^{-23}	3.393	1530

[a] Estimated uncertainty factor is 1.35 for overall rate constants, k_1 and k_2 in the specified temperature range.

contains the change of the C−H−O angle, becomes smaller than that in the OH + benzene transition state, and a relatively large vibrational frequency is calculated (266 cm^{-1} by B3LYP/6-31G(d)). This significantly reduces the partition function of the mode, and the effect of anharmonicity to the total partition function becomes much smaller. A similar reduction of the effect of anharmonicity is also expected for the alkane hydrocarbons with many loose torsion vibrational modes, though the precise theoretical investigations based on the reliable experimental rate constants is needed for further assessment of the possible effect of anharmonicity. The effect of the anharmonicity of C−H−O bending in the transition state is expected to be most prominent in the H-abstraction reactions from a tight molecule like benzene, and similar ring H abstractions from aromatic hydrocarbons.

F. Recommended Rate Constants. On the basis of the TST fit of the experimental results, the recommended overall rate constants for reactions 1 and 2, as well as the rate constants for each channel, are listed in Table 2. The estimated uncertainty factor is 1.35 for the overall rate constants, k_1 and k_2, which have been measured directly in the present and previous studies; while the rate constants for minor channels, such as substitution channel, should deserve a larger uncertainty factor as large as 2, since they depend significantly on the estimated energies.

Conclusions

The direct measurements of the high-temperature rate constants for the reactions of OH radicals with benzene and toluene have been extended up to 1740 and 1480 K, respectively, and were in good agreement with the previous measurements. Theoretical investigations were also extended in order to resolve the disagreement between the TST calculations and experiments, and the anharmonicity of the C−H−O bending vibrations was found to be essential in order to reproduce the experimental rate constants by TST. The energetics of the possible channels have been estimated on the basis of the quantum chemical calculations, experimental information, and the previous theoretical investigations, and the dominant channels were confirmed to be the H-atom abstraction channel for OH + benzene and the methyl H-abstraction channel for OH + toluene in the present experimental temperature range.

Acknowledgment. Authors thank Dr. Joe V. Michael (Argonne National Laboratory) for his useful discussions and comments in regard to the development of our new apparatus and kind comments and suggestions to this work. We are thankful to Prof. Hiroyuki Matsui (Toyohashi University of Technology) for his continued encouragement to our work.

Supporting Information Available: Tables 1S and 2S contain the reaction mechanisms used in the kinetic numerical simulations. Table 3S shows the measured rate constants for OH + benzene/toluene with the experimental conditions. Tables 4S and 5S and Figures 1S and 2S show the results of quantum chemical calculations used in TST calculations. Table 6S shows the comparison of experimental and calculated entropies and heat capacities. This material is available free of charge via the Internet at http://pubs.acs.org.

References and Notes

(1) Atkinson, R. *Chem. Rev.* **1986**, *86*, 69.
(2) Atkinson, R. *J. Phys. Chem. Ref. Data* **1989**, Monograph 1.
(3) Atkinson, R. *J. Phys. Chem. Ref. Data* **1994**, Monograph 2.
(4) Perry, R. A.; Atkinson, R.; Pitts, J. N., Jr. *J. Phys. Chem.* **1977**, *81*, 296.
(5) Lorenz, K.; Zellner, R. *Ber. Bunsen-Ges. Phys. Chem.* **1983**, *87*, 629.
(6) Bourmada, N.; Devolder, P.; Sochet, L. R. *Chem. Phys. Lett.* **1988**, *149*, 339.
(7) Knispel, R.; Koch, R.; Siese, M.; Zetzsch, C. *Ber. Bunsen-Ges. Phys. Chem.* **1990**, *94*, 1375.
(8) Markert, F.; Pagsberg, P. *Chem. Phys. Lett.* **1993**, *209*, 445.
(9) Semadeni, M.; Stocker, D. W.; Kerr, J. A. *Int. J. Chem. Kinet.* **1995**, *27*, 287.
(10) Lay, T. H.; Bozzelli, J. W.; Seinfeld, J. H. *J. Phys. Chem.* **1996**, *100*, 6543.
(11) Anderson, P. N.; Hites, R. A. *Environ. Sci. Technol.* **1996**, *30*, 301.
(12) Bjergbakke, E.; Sillesen, A.; Pagsberg, P. *J. Phys. Chem.* **1996**, *100*, 5729.
(13) Kramp, F.; Paulson, S. E. *J. Phys. Chem. A* **1998**, *102*, 2685.
(14) Bohn, B.; Zetzsch, C. *Phys. Chem. Chem. Phys.* **1999**, *1*, 5097.
(15) Bohn, B. *J. Phys. Chem. A* **2001**, *105*, 6092.
(16) Berndt, T.; Boge, O. *Phys. Chem. Chem. Phys.* **2001**, *3*, 4946.
(17) Birger, B. *J. Phys. Chem. A* **2001**, *105*, 6092.
(18) Johnson, D.; Raoult, S.; Rayez, M. T.; Rayez, J. C.; Lesclaux, R. *Phys. Chem. Phys. Chem.* **2002**, *4*, 4678.
(19) Volkamer, R.; Klotz, B.; Barnes, I.; Imamura, T.; Wirtz, K.; Washida, N.; Becker, K. H.; Platt, U. *Phys. Chem. Chem. Phys.* **2002**, *4*, 1598.
(20) Albarran, G.; Bentley, J.; Schuler, R. H. *J. Phys. Chem. A* **2003**, *107*, 7770.

(21) Anderson, R. S.; Czuba, E.; Ernst, D.; Huang, L. Thompson, A. E.; Rudolph, J. *J. Phys. Chem. A* **2003**, *107*, 6191.
(22) Raoult, S.; Rayez, M. T.; Rayez, J. C.; Lesclaux, R. *Phys. Chem. Chem. Phys.* **2004**, *6*, 2245.
(23) Lin, S. C.; Kuo, T. C.; Lee, Y. P. *J. Chem. Phys.* **1994**, *101*, 2098.
(24) Tully, F. P.; Ravishanka, A. R.; Thompson, R. L.; Nicovich, J. M.; Shah, R. C.; Kreuffer, N. M.; Wine, P. H. *J. Phys. Chem.* **1981**, *85*, 2262.
(25) Madronich, S.; Felder, W. *J. Phys. Chem.* **1985**, *89*, 3556.
(26) Baulch, D. L.; Cobos, C. J.; Cox, R. A.; Esser, C.; Frank, P.; Just, Th.; Kerr, J. A.; Pilling, M. J.; Troe, J.; Walker, R. W.; Warnatz, J. *J. Phys. Chem. Ref. Data* **1992**, *21*, 411.
(27) Baulch, D. L.; Cobos, C. J.; Cox, R. A.; Frank, P.; Hayman, G.; Just, Th.; Kerr, J. A.; Murrells, T.; Pilling, M. J.; Troe, J.; Walker, R. W.; Warnatz, J. *J. Phys. Chem. Ref. Data* **1994**, *23*, 847.
(28) Tokmakov, I. V.; Lin, M. C. *J. Phys. Chem. A* **2002**, *106*, 11309.
(29) Chen, C. C.; Bozzelli, J. W.; Farrell, J. T. *J. Phys. Chem. A* **2004**, *108*, 4632.
(30) Suh, I.; Zhang, D.; Zhang, R.; Molina, L. T.; Molina, M. J. *Chem. Phys. Lett.* **2002**, *364*, 454.
(31) Seta, T.; Nakajima, M.; Miyoshi, A. *Rev. Sci. Instrum.* **2005**, *76*, 064103.
(32) Benson, S. W.; Spokes, G. N. *J. Phys. Chem.* **1968**, *72*, 1182.
(33) Stern, S. A.; Mullhaupt, J. T. *Chem. Rev.* **1960**, *60*, 185.
(34) Harrison, H.; Johnston, H. S.; Hardwick, E. R. *J. Am. Chem. Soc.* **1962**, *84*, 2478.
(35) Chakraborty, D.; Park, J.; Lin, M. C. *Chem. Phys.* **1998**, *231*, 39.
(36) Wooldridge, M. S.; Hanson, R. K.; Bowman, C. T. *Int. J. Chem. Kinet.* **1994**, *26*, 389.
(37) Bott, J. F.; Cohen, N. *Int. J. Chem. Kinet.* **1991**, *23*, 1017.
(38) De Avillez Pereira, R.; Baulch, D. L.; Pilling, M. J.; Robertson, S. H.; Zeng, G. *J. Phys. Chem. A* **1997**, *101*, 9681.
(39) Baboul, A. G.; Curtiss, L. A.; Redfern, P. C.; Raghavachari, K. *J. Chem. Phys.* **1999**, *110*, 7650.
(40) Montgomery, J. A., Jr.; Frisch, M. J.; Ochterski, J. W.; Peterson, G. A. *J. Chem. Phys.* **1999**, *110*, 2822. (b) Montgomery, J. A., Jr.; Frisch, M. J.; Ochterski, J. W.; Peterson, G. A. *J. Chem. Phys.* **2000**, *112*, 6532.
(41) Frisch, M. J.; Trucks, G. W.; Schlegel, H. B.; Scuseria, G. E.; Robb, M. A.; Cheeseman, J. R.; Montgomery, J. A., Jr.; Vreven, T.; Kudin, K. N.; Burant, J. C.; Millam, J. M.; Iyengar, S. S.; Tomasi, J.; Barone, V.; Mennucci, B.; Cossi, M.; Scalmani, G.; Rega, N.; Petersson, G. A.; Nakatsuji, H.; Hada, M.; Ehara, M.; Toyota, K.; Fukuda, R.; Hasegawa, J.; Ishida, M.; Nakajima, T.; Honda, Y.; Kitao, O.; Nakai, H.; Klene, M.; Li, X.; Knox, J. E.; Hratchian, H. P.; Cross, J. B.; Adamo, C.; Jaramillo, J.; Gomperts, R.; Stratmann, R. E.; Yazyev, O.; J. Austin, A.; Cammi, R.; Pomelli, C.; Ochterski, J. W.; Ayala, P. Y.; Morokuma, K.; Voth, G. A.; Salvador, P.; Dannenberg, J. J.; Zakrzewski, V. G.; Dapprich, S.; Daniels, A. D.; Strain, M. C.; Farkas, O.; Malick, D. K.; Rabuck, A. D.; Raghavachari, K.; Foresman, J. B.; Ortiz, J. V.; Cui, Q.; Baboul, A. G.; Clifford, S.; Cioslowski, J.; Stefanov, B. B.; Liu, G.; iashenko, A.; Piskorz, P.; Komaromi, I.; Martin, R. L.; Fox, D. J.; Keith, T.; Al-Laham, M. A.; Peng, C. Y.; Nanayakkara, A.; Challacombe, M.; Gill, P. M. W.; Johnson, B.; Chen, W.; Wong, M. W.; Gonzalez, C.; Pople, J. A. *Gaussian 03*, revision B.03; Gaussian, Inc.: Pittsburgh, PA, 2003.
(42) Chase, M. W., Jr.; Davles, C. A.; Downey, J. R., Jr.; Frurip, D. J.; McDonald, R. A.; Syverud, A. N. JANAF Thermochemical Tables, 3rd ed.; *J. Phys. Chem. Ref. Data* **1985**, *14*, Supplement 1.
(43) Frenkel, M.; Marsh, K. N.; Wilhoit, R. C.; Kabo, G. J.; Roganov, G. N. *Thermodynamics of Organic Compounds in the Gas State*; Thermodynamic Research Center: College Station, TX, 1994; Vols I and II.
(44) Tsang, W. *Heats of Formation of Organic Free Radicals by Kinetic Methods in Energetics of Organic Free Radicals*; Martinho Simoes, J. A., Greenberg, A., Liebman, J. F., Eds.; Blackie Academic and Professional: London, 1996; p 22.
(45) Ruscic, B.; Wagner, A. F.; Harding, L. B.; Asher, R. L.; Feller, D.; Dixon, D. A.; Peterson, K. A.; Song, Y.; Qian, X.; Ng, C.-Y.; Liu, J.; Chen, W.; Schwenke, D. W. *J. Phys. Chem. A* **2002**, *106*, 2727. (b) Herbon, J. T.; Hanson, R. K.; Golden, D. M.; Bowman, C. T. *Proc. Combust. Inst.* **2002**, *29*, 1201.
(46) Ruscic, B.; Litorja, M.; Asher, R. L. *J. Phys. Chem. A* **1999**, *103*, 8625; **2000**, *104*, 8600 (correction).
(47) Davico, G. E.; Bierbaum, V. M.; DePuy, C. H.; Ellison, G. B.; Squires, R. R. *J. Am. Chem. Soc.* **1995**, *117*, 2590.
(48) Greenwald, E. E.; North, S. W.; Georgievskii, Y.; Klippenstein, S. J. *J. Phys. Chem. A* **2005**, *109*, 6031.
(49) Pitzer, K. S.; Gwinn, W. D. *J. Chem. Phys.* **1942**, *10*, 428.
(50) Huber, K. P.; Herzberg, G. *Molecular Spectra and Molecular Structures*, *IV. Constants of Diatomic Molecules*; Van Nostrand Reinhold: New York, 1979.
(51) Eckart, C. *Phys. Rev.* **1930**, *35*, 1303. (b) Garrett B. C.; Truhlar, D. G. *J. Phys. Chem.* **1979**, *83*, 2621.
(52) Pitzer, S. K. *J. Chem. Phys.* **1946**, *14*, 239.
(53) See http://www.frad.t.u-tokyo.ac.jp/~miyoshi/tools4kin.html.
(54) Gilbert, R.; Smith, S. C. *Theory of Unimolecular and Recombination Reactions*; Blackwell: Oxford, 1990.
(55) Garrett, B. C.; Truhlar, D. G. *J. Phys. Chem.* **1979**, *83*, 1915. (b) Tokmakov, I. V.; Park, J.; Gheyas, S.; Lin, M. C. *J. Phys. Chem. A* **1999**, *103*, 3636.